Observation of annular electron beam transport in multi-TeraWatt laser-solid interactions

J S Green, K L Lancaster, P A Norreys

Central Laser Facility, CCLRC Rutherford Appleton Laboratory, Chilton, Didcot, Oxon., OX11 0QX, UK

M Tatarakis, M S Wei, A E Dangor, K Krushelnick

Blackett Laboratory, Imperial College London, Price Consort Road, London SW7 2BZ, UK

E L Clark

Plasma Physics Division, AWE plc, Aldermaston RG7 4PR, UK

J R Davies

GoLP, Instituto Superior Tecnico, Lisbon, Portugal

M Zepf

Department of Pure & Applied Physics, Queens University Belfast, Belfast BT7 1NN, UK

Main contact email address: *j.s.green@rl.ac.uk*

Introduction

The study of fast electron energy transport with current densities in the range 10^{12} A cm^{-2} is a fascinating subject in its own right and one that also has important implications for applications of ultra-high intensity lasers, for example in the optimisation of proton and heavy ion acceleration processes[1)], hot spark formation in fast ignition[2)] and in dense plasma radiography for inertial confinement fusion[3)].

This field of study has grown rapidly since the first measurements of energy transport of electron beams generated by multi-TW laser pulses showing collimated electron flow patterns in both deuterated plastic targets[4)] and large area glass slabs[5)].

In experiments at the Vulcan 100 TW facility a K_α imaging technique was used to image photons emitted as a result of K-shell ionization by fast electrons created in a 20μm thick buried Ti or Cu fluor layer in a planar Al or CH target. This permitted the observation of the transverse dimension of the laser-generated electron beam and the results indicated that the K_α source size was always larger than the focal spot dimensions and that the electron beam diverged with an angular spread of 40° [6)].

We report here on electron energy transport experiments conducted on the Vulcan 100 TW laser facility with large area thick foil targets that provide new insight into electron transport in low Z targets. For plastic targets it is shown, by the plasma expansion measured in shadowgrams taken after the interaction pulse, that there is a transition between previously reported collimated electron flows at 10 TW to an annular electron flow pattern with a 20° divergence angle for peak powers of ~70 TW. Intermediate powers on target suggest that both the central collimated flow pattern and the annular structure co-exist.

Experiment

The experiments described here were conducted on the Vulcan 100 TW laser facility[7)]. This laser delivered up to 120 J in a pulse of 0.9 – 1.1 ps duration to target in a focal spot diameter of 10 μm by a 60 cm focal length, F/4.2 off-axis parabola. 35% of the laser energy was contained within the focal spot and corresponded to a peak intensity of up to 5×10^{19} W cm^{-2}. The intensity contrast ratio was 10^{-7}. The laser wavelength was 1054nm. The p-polarised laser radiation was incident onto target at 45° angle of incidence. The targets were large area foils of Mylar.

Plasma expansion on the front and rear of the heated target was obtained from shadowgrams using a $2\omega_0$ optical probe that was passed transversely across the target surface 200ps after the interaction pulse. The image plane was relayed outside the target chamber to an 8-bit charge couple device (CCD) which digitized and recorded the shadowgrams onto a computer. Refraction of the probe light in the large density gradients limited the observations to regions with electron densities less than 10^{20} cm^{-3}.

To obtain information on the proton beam pattern emerging from the rear of the target (that provides qualitative information on the electron transport pattern inside the solid density plasma) a stack of Gafchromic MD-55 radiochromic film interleaved with CR-39 plastic nuclear track detectors was deployed. The CR-39 is only sensitive to protons (as no other ions are expected to penetrate through the first layer of radiochromic film) and this allows one to distinguish proton features from electron and X-ray features in the radiochromic film layers. The proton energy required to penetrate the stack increases with depth and the spatially resolved pattern provides a measurement of the proton beam at particular energies.

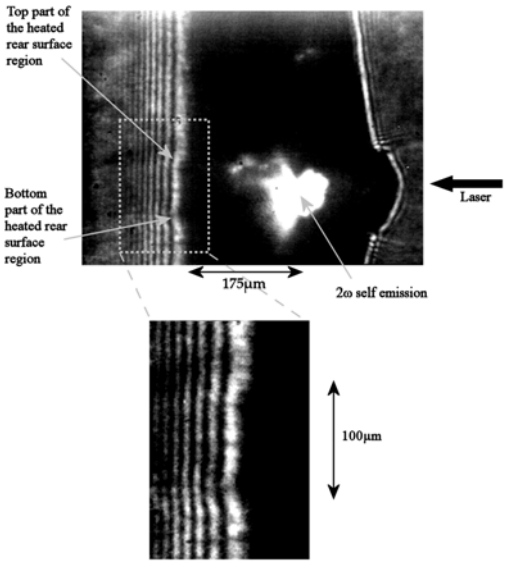

Figure 1. A 26TW laser pulse incident onto a 175μm thick mylar target, corresponding to an intensity of 1×10^{19} Wcm^{-2} within the focal spot. The heated plasma on the rear surface of the target is uniform within a 20° divergence angle**.**

Results

Figures 1 - 3 show a series of shadowgrams of 5 mm × 5 mm 175 μm thick Mylar foils taken 200 ps after the main interaction pulse with laser powers of 26 TW, 50 TW and 68 TW, respectively. The location of the interaction point in all images

is provided by the self-generated $2\omega_0$ emission that is generated by the relativistic oscillations of the critical density surface. The plasma expansion of the hot region of the front surface of the target can be observed in all cases, but of particular interest is the rear surface plasma expansion.

The rear surface expansion patterns indicate a global 20° full-width at half maximum (FWHM) divergence angle in all cases, but the structure of the profiles changes as the intensity on target rises. Figure 1 shows a uniformly heated pattern within the 20° divergence angle. Figure 2 shows both the central collimated flow pattern observed previously with 10 TW laser pulses[4] surrounded by an annular structure. Figure 3 shows that the central collimated feature has disappeared and only the annular structure remains.

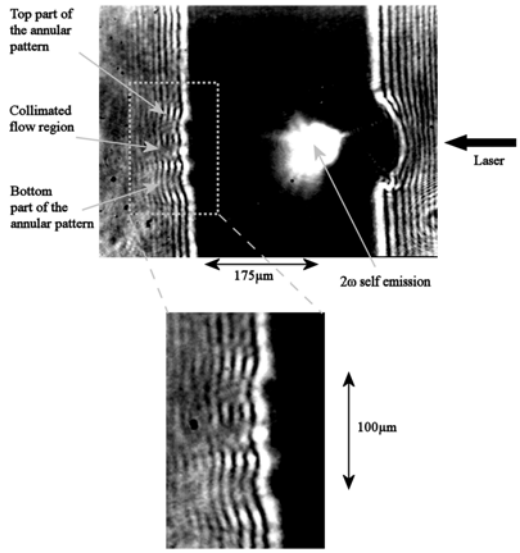

Figure 2. A 50TW laser pulse on a 175μm thick mylar target, corresponding to an intensity of 2×10^{19} Wcm^{-2} within the focal spot. The heated plasma on the rear surface of the target exhibits a central heated region surrounded by an annular structure with a total divergence angle of 20°.

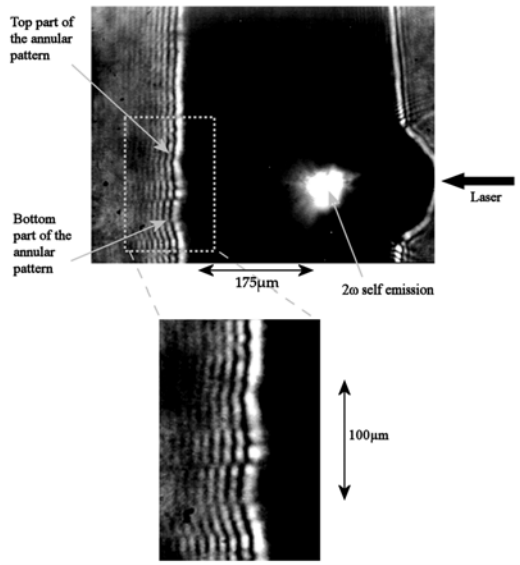

Figure 3. A 68TW laser pulse on a 175μm thick mylar target, corresponding to an intensity of 3×10^{19} Wcm^{-2} within the focal spot. The heated plasma on the rear surface of the target is now annular in shape. The central heated region is not distinguishable within the annular pattern.

The inference from the shadowgrams of an annular structure on the rear surface of the target can be explained by the way in which the probe beam behaves when passing through such a structure. Figure 4 presents a simplified schematic of such a process. Light rays that do not pass through any plasma are not deflected, forming the bright field on the shadowgram. A light ray passing through annular structure would be deflected in proportion to the total distance travelled through the plasma. The ray is deflected by an angle θ over a small path length *dl* by the relation:

$$\theta = \nabla_{\perp} \int \eta \, dl$$

where η is the refractive index of the plasma defined by:

$$\eta = (1 - n_e/n_c)^{1/2}$$

where n_e is the electron density and n_c is the critical density. Hence the rays at points **b** and **c** that pass through the longest length of plasma are deflected to a greater extent than ray **a**. This would result in a "double hump" pattern as seen on the experimentally obtained images.

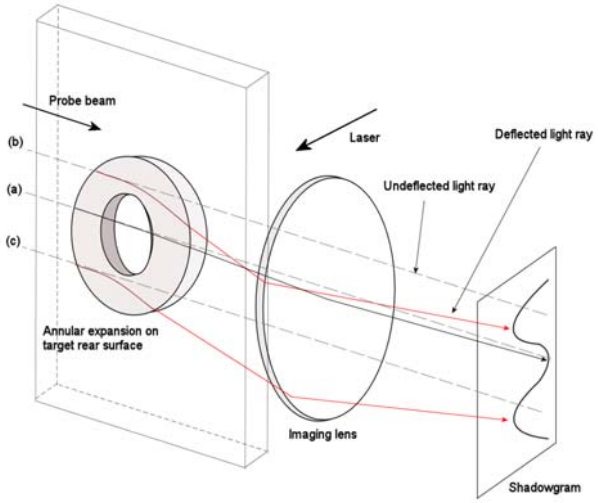

Figure 4. Schematic of how a typical shadowgram would be formed from the propagation of a probe beam through an annular expansion on the rear surface of the target.

Two possible interpretations of these observations require discussion. The first is that these features are the result of large-scale filamentation of the fast electron beam within the target that manifest themselves as local heating on the rear surface. However, the observations are contrary to this hypothesis, as these features would appear randomly within the observed 20° divergence pattern. The expansion features on the rear surface in the shadowgrams were consistently observed in the same position relative the interaction region. The second is that they are the result of a fountain field on the rear surface that locally heats the plasma where the fast electron beam re-enters the target. Three dimensional particle-in-cell simulations[8] indicate that a central heated column is formed by the fast electron beam propagation in the over-dense plasma and the fountain field is formed when the target potential reaches a level that prevents fast electron propagation into the vacuum. This is inconsistent with the observations because the annular structure should always be accompanied by a jet of plasma arising from the central heated region, which is clearly not always the case.

Nevertheless, small-scale filamentation of the fast electron beam is confirmed by measurements of the MeV proton pattern from the rear surface of the targets recorded in radio-chromic film. Figure 5 shows a typical example of the observed beam pattern. Each layer of radio-chromic film corresponds to a particular stopping range of the proton beam. The proton beam is non-relativistic and therefore the patterns recorded at different depths in the detector stack correspond to different time zones in the proton beam evolution[9]. At 26 MeV, corresponding to the earliest time, a distorted annular ring

pattern is observed within a 10° divergence angle. At 25MeV, one begins to observe the formation of a fine-scale filamentary structure that becomes much more pronounced at 17MeV within a 20° divergence angle. The filamentary structure is no longer observed with lower energy components of the proton beam at 3MeV. Since the proton beam is formed from a combination of shock formation at the front surface and sheath acceleration from the rear surface[10], the data suggests that the fast electron propagation inside the solid density plasma at later times is smoother, i.e. the filamentation process is no longer affecting the fast electron beam propagation.

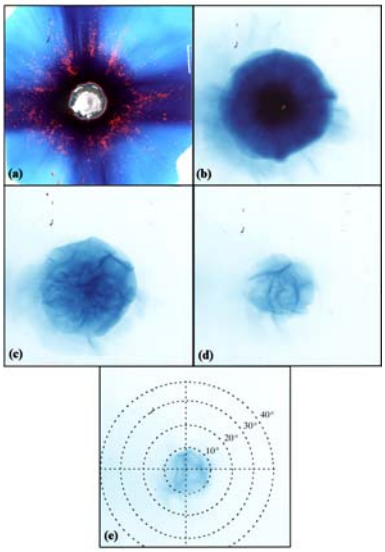

Figure 5. Radiochromic film images at different depths in the detector stack. Each layer has a proton beam energy of (a) ≥ 100keV (b) ≥ 3MeV (c) ≥ 17MeV (d) ≥ 25MeV and (e) ≥ 26MeV. Fine scale filamentary structure within the beam is visible, particularly in images (c) and (d). The filamentary structure is not visible in image (b).

Discussion

Beam hollowing in the plastic targets could be caused by: (i) a filamentation instability with a wavelength equal to the diameter of the beam, (ii) evolution towards a hollow equilibrium state and (iii) reversal of the magnetic field due to the fall in target resistivity caused by Ohmic heating. Mechanism (i) does not appear to be consistent with the observations because shorter wavelength modes and other instabilities, such as 2-stream and hosing, would also be expected to occur[11]. Hollowing has been reported by Taguchi *et al.* [12], but they considered a beam with a radius comparable to the skin depth so it could only support this filamentation mode. The apparent absence of such instabilities is most likely due to the high collision frequency in the solid and a high beam temperature. Mechanism (ii) could occur if the beam temperature were higher on-axis[13], which may well occur due to the higher laser intensity on-axis. This is apparent from a consideration of the pressure gradient. Calculations of such equilibria including the magnetic field have been given by Hammer and Rostoker[13] and by Gratreau[14]. However, it appears unlikely that an equilibrium state would ever be reached and there is no reason for such a mechanism to have a distinct intensity threshold.

Mechanism (iii) has been considered by Davies[15] with a simple analytical model that uses the rigid beam model and Ohm's law for the target, including the change in resistivity due to Ohmic heating. This depends on the square of the current density, so the electric field changes from increasing with current density to decreasing with current density if the resistivity falls faster than linearly with temperature, which would be expected to occur since the Spitzer resistivity applies at high temperatures. The resulting change in the gradient of the electric field leads to a change in the sign of the magnetic field generation and eventually to a reversal of the magnetic field, which would cause the beam to hollow rather than to pinch. Davies estimated that minimum average intensities of the order of 10^{19} W cm^{-2} would be required for this to occur. Beam hollowing can indeed be seen in the numerical modelling of similar experiments at such an average intensity[16] described by Davies *et al.*[17], although it cannot be seen in the time-integrated plots of electron energy reflected from the back surface because of the magnetic focusing that they describe. Beam hollowing would be more difficult to obtain in metals because a lot more energy is required to get a large fall in the resistivity and this occurs at a higher temperature. Also, metals have a higher heat capacity than plastic. As a result of the complexity of the situation and uncertainties as to the actual beam and target parameters it is not possible to give a meaningful, quantitative comparison with Davies' model, it can merely be stated that the observed intensity threshold is consistent with this mechanism.

Summary

In summary, it has been shown, by plasma expansion measured in shadowgrams taken after the interaction pulse, that there is a transition between previously reported collimated electron flows at 10TW to an annular electron flow pattern with a 20° divergence angle for peak powers at ~70TW. Intermediate powers on target suggest that both the central collimated flow pattern and the annular structure can co-exist. The evolution of the proton beam pattern from the rear surface of plastic targets recorded in radio-chromic film images indicates that after the initial annular structure is formed, fine-scale filamentation of the fast electron flow occurs, becomes more pronounced but is then later smoothed out. These measurements are consistent with the Davies rigid beam model for fast electron flow.

References

1. E L Clark *et al.*, Phys. Rev. Lett. 84, 670 (2000); R A Snavely *et al.*, Phys. Rev. Lett. 84, 2945 (2000); E L Clark *et al.*, Phys. Rev. Lett.85, 1654 (2000)
2. M Tabak *et al.*, Phys. Plasmas 1, 1626 (1994)
3. R D Edwards *et al.*, Appl. Phys. Lett. 80, 2129 (2002)
4. M Tatarakis *et al.*, Phys. Rev. Lett. 81, 999 (1998)
5. M Borghesi *et al.*, Phys. Rev. Lett. 81, 112 (1998)
6. R B Stephens *et al.*, Phys. Rev. E 69, 066414 (2004)
7. C N Danson *et al.*, J. Modern Optics., 45, 1653 (1998)
8. A Pukhov Phys. Rev. Lett. 86, 3562 (2002)
9. M Borghesi *et al.*, Plasma Phys. Controlled Fusion 43, A267 (2001)
10. M Zepf *et al.*, Phys Rev. Lett. 90, 064801 (2003)
11. L O Silva *et al.*, Phys. Plasmas 9, 2458 (2002); A Bret *et al.*, Phys. Rev. Lett. 94, 115002 (2005); L Gremillet, *et al.*, Phys. Plasmas 9, 941 (2002).
12. T Taguchi *et al.*, Phys. Rev. Lett 86, 5055 (2001); T Taguchi *et al.*, Comp. Phys. Commun. 164, 269 (2004)
13. D A Hammer and N Rostoker, Phys. Fluids 13, 1831 (1970)
14. P Gratreau, Phys. Fluids 21, 1302 (1978).
15. J R Davies, Phys. Rev. E 68, 056404 (2003).
16. M Tatarakis, *et al.*, Phys. Rev. Lett. 81, 999 (1998).
17. J R Davies, A R Bell and M Tatarakis, Phys. Rev. E 59, 6032 (1999).